HHS Public Access

Author manuscript

Vision Res. Author manuscript; available in PMC 2021 February 01.

Published in final edited form as:

Vision Res. 2020 February ; 167: 15–23. doi:10.1016/j.visres.2019.12.005.

Genetic dissection of rod and cone pathways mediating light responses and receptive fields of ganglion cells in the mouse retina

RL Seilheimer, **J Sabharwal**, **SM Wu**

Cullen Eye Institute, Baylor College of Medicine, Houston, TX 77030,

Abstract

Retinal ganglion cells (GCs) are important visual neurons which carry complex spatiotemporal information from the retina to higher visual centers in the brain. By taking advantage of pathway-specific knockout/mutant mice and multi-electrode array (MEA) recording techniques, we analyze contributions of rod and cone pathways to responsiveness, kinetics and receptive field profiles of GCs under scotopic and photopic conditions. Our data suggest: (1) Scotopic responses of some GCs require all three rod pathways, some require only the secondary and tertiary rod pathways, and others require only the tertiary rod pathway. (2) There are more responsive GCs in photopic conditions than responsive GCs in scotopic conditions. (3) Gap junctions slow down GCs' scotopic light responses and increase GCs' ratio of antagonistic to center inputs. (4) Cone pathways do not affect the kinetics but alter the ratio of antagonistic to center inputs of scotopic GC responses, and they speed up GCs photopic responses and alter the ratio of GCs' antagonistic to center synaptic inputs and receptive field profiles. (5) Rod bipolar cells shorten response latency of ON GCs and increase the ratio of GCs' antagonistic to center synaptic inputs. (6) Light adaptation speeds up GCs' temporal processing and tunes GC photopic responses to higher frequencies, and the tertiary rod pathway plays a significant role in adaptation-induced TTP changes in some GCs. (7) GC RF center sizes are partially mediated by AIIACs and GC-GC coupling. (8) Connexin36 gap junctions and cone pathways alter synaptic circuits underlying antagonistic surround inputs to GCs in photopic conditions.

Keywords

Retinal ganglion cells; AII amacrine cells; light-evoked spike responses; spike triggered average (STA); receptive field center; receptive field surround

Correspondance: Samuel M. Wu, Ph.D., Cullen Eye Institute, Baylor College of Medicine, One Baylor Plaza, NC-205, Houston, TX 77030. Tel: 713-798-5966, Fax: 713-798-6457, swu@bcm.edu.

Seilheimer RL and Sabharwal J. performed the MEA recordings and data analysis, and Wu SM performed data analysis and wrote the manuscript.

1. Introduction

Ganglion cells (GCs) are the output neurons of the retina, and mammalian GCs can be classified into over 20 morphological types [1–3]. Rod and cone inputs to these GCs are mediated by 10 types of bipolar cells (BCs) and over 30 types of amacrine cells (ACs). While conventional wisdom has it that mammalian rods and cones make segregated contacts with respective rod and cone BCs [4,5], we and others have found that a subpopulation of rod bipolar cells receive direct synaptic inputs from cones and likewise subpopulations of cone bipolar cells get direct synaptic inputs from rods [6–9]. These novel wiring schemes and the diversity of retinal neurons warrant detailed investigations to reveal how specific rod and cone signaling pathways are used to relay visual information through the retina. Factoring in the fact that rods and cones, as well some ACs, BCs and some GCs are electrically coupled through gap junctions [10–13], Figure 1 summarizes the current knowledge of rod and cone synaptic pathways that feed into ON and OFF GCs in mammalian retinas. One exclusive feature of the mammalian retina is that its rod BCs lack direct synapses onto GCs but onto AII amacrine cells (AIIACs) instead, which make electrical synapses with ON cone BCs [14,15], that send signals to ON GCs; and inhibitory glycinergic synapses on OFF BCs and OFF GCs [16–18]. These synaptic circuits have been named the *primary* rod pathway (pathway 1 in Figure 1A). Rod signals can also be transmitted to GCs via rod-cone gap junctions, subsequently to ON and OFF cone BCs, then to ON and OFF GCs in the so-called *secondary* rod pathway [10,11,19] (pathway 2 in Figure 1A). We and others described the *tertiary* rod pathway in which rod signals are transmitted to ON and OFF cone BCs by direct chemical synapses [6–9]. The *primary* cone pathway is defined as direct chemical synapses from cones to cone BCs and to GCs (pathway 1’ in Figure 1B), and the *secondary* cone pathway is the cone-to-rod gap junction-mediated signaling circuits (pathway 2’ Figure 1B). As a reverse of the rod tertiary pathway, cones make direct synapses onto a subpopulation of rod BCs, which send signals to the AIIAC circuits [6] (*tertiary* cone pathway 3’ in Figure 1B). It has been shown that subpopulations of mammalian GCs are electrically coupled, and connexin36 is found to mediate some GC-GC coupling (pathway 4 in Figure 1) [20].

In this study, we examined how these rod and cone pathways affect the spatiotemporal response profiles of various types of GCs by taking advantage of pathway-specific knockout/mutant mouse lines: $Trα^{-/-}$ *(aka Gnat1*−/−, lacking rod signals) [21], $Gnat2^{cplf3}$ (lacking cone signals) [22], $Cx36^{-/-}$ (lacking rod-cone coupling and AIIAC coupling) [10,14], and $Bhlhb4^{-/-}$ (lacking rod-bipolar cells) [23]. Rod and cone signaling pathways suppressed in each of the four mutant mice are marked by “X” of four colors in Figure 1. We analyzed the GCs’ responsiveness, spike response kinetics, and center and surround receptive field profiles under scotopic (rod mediated) and photopic (cone-mediated) conditions in these mouse lines, by using the multi-electrode array (MEA) recording technique in conjunction with white-noise checkerboard stimulation and spike triggered average methods [24,25]. By comparing response parameters obtained from each mutant mouse line with the corresponding parameters obtained in the wildtype mice, we are able to determine the contribution of various rod and cone pathways to the spatiotemporal response profiles of ON and OFF GCs.

2. Materials and Methods:

2.1. Preparations and multielectrode array (MEA) recording

The wildtype mouse used was C57Black6J from Jackson laboratory (Bar Harbor, Maine). Generation of mutants has been described in previous publications [10,21–23], and the *Tra*−/−, *Gnat2*^{cplf3}, *Cx36*−/− and *Bhlhb4*−/− mice have been bred and used in our laboratory for 8–13 years [6,7,14,19]. All animals were handled in accordance with Baylor College of Medicine's policies on the treatment of laboratory animals and conform to the ARVO Statement on the Use of Animals in Ophthalmic and Vision Research and the NIH guide for the Use of Laboratory Animals. Mice were dark-adapted for 1–2 hours prior to the experiment, and dissection procedures have been described in previous publications [16,24–26]. In brief, eyes were removed under infrared illumination using night vision scopes (Nitemare, BE Meyers, Oregon) and whole-mount retinas were placed onto a multielectrode array, ganglion cell side down. Recordings were made primarily from central retina. The multielectrode array (MEA-60, Multichannel Systems, Tübingen Germany) had 60 electrodes spaced 100 μm apart, each with a diameter of 10 μm. Ganglion cell action potentials were recorded at 20 KHz and pre-filtered with a 0.1 Hz high-pass hardware filter.

2.2. Solutions

The retina was kept at 35.6° C and perfused with carboxygenated (95% O_2, 5% CO_2) recording solution (in mM: NaCl, 124; KCl, 2.5; $CaCl_2$, 2; $MgCl_2$, 2; NaH_2PO_4, 1.25; $NaHCO_3$, 26; and glucose, 22 at pH 7.35) (Tian and Copenhagen, 2003). Experiments were first performed in the standard (control) recording solution, and then with 2 μM strychnine mixed into the solution. In some experiments, additional recordings were performed in standard recording solution after the drug was washed out.

2.3. Spike sorting

Potential spikes were identified from each recording as signals greater than 3 standard deviations from baseline. These were sorted using a clustering algorithm (Kadir et al., 2014), based on key features for the waveform of each spike. These features included spike amplitude, spike shape, and the electrical footprint. The electrical footprint was identified as the activity on every other channel during each potential spike, thus outlining a shape of the axon for each cell. Each potential unit from this clustering method was assessed for contamination based on a ratio of the firing rate within the refractory period to the overall firing rate of the cell [25].

2.4. Light stimulation

Similar to our previous report (Cowan et al., 2016a) and those of others (Pandarinath et al., 2010b), the ambient white light level during an experiment was measured as wavelength specific irradiance (E(λ), in microwatts cm^{-2}) in the plane of the preparation (Thor Labs, S170C and Edmund Optics, SpectraRad). The mean ambient photopic light level was 757.9 R*/rod/sec and the monitor had a contrast of −1 to 1. Neutral density filters were used to create three log unit attenuation, creating an ambient scotopic light level of 0.8 R*/rod/sec. Stimuli were projected as an optically reduced image from a computer monitor which

presented light from the visible spectrum (Dell, SXGA-JF311–5100). A beam splitter was used to present the image from the computer monitor from below the MEA. Whole field light steps are non-linear stimulation that delivered 30 repeated trials of 4 seconds of a black screen followed by 4 seconds of a white screen to the retina. The spike response to whole-field light step (SRWFLS) stimulation scheme sorted RGCs into five functional groups (see above). Linear receptive fields (RF) were mapped using random binary white noise checkerboards presented at 15 Hz. Each square in the checkerboard was either black or white and 50μm on a side. The stimulus was created and presented with PsychToolbox (Brainard, 1997; Pelli, 1997). Reverse correlation was used to compute a space-time spike-triggered average (STA) (Meister et al., 1994; Chichilnisky, 2001).

2.5. Spatial pooling and surround characterization

The STA was first fit to the product of a spatial Gaussian and the impulse response of a temporal filter (Chichilnisky and Kalmar, 2002). The spatial Gaussian determines the size of the 1-σ distance in the major and minor axis. This was used to determine 1-σ annular zones. Temporal traces within zones 1–3 were combined to form a single center trace while those in zones 4–9 were combined to form a surround trace. By summing the first 150 ms of the center and surround trace we identified a single value to characterize the center and surround. The ratio of these values (surround/center) was calculated and is reported in this report as the Surround Polarity Index (SPI) (Cowan et al., 2016a). A negative value indicates opposite polarity of the center and surround. A larger absolute value indicates a stronger surround.

2.6. White noise checkerboard stimuli for spatiotemporal receptive field measurements

A white noise stimulus composed of a two-dimensional array (a 32×32 checkerboard) of squares (pixels), each flickering randomly and independently at 15 Hz was used to study the spatiotemporal properties of GCs recorded with the MEA. The white noise (random) checkerboard stimulus was presented with a computer monitor. The mean photopic level is set at 5,000 R* rod^{-1} sec^{-1}, and the mean scotopic level is set at 5 R* rod^{-1} sec^{-1} with a −3 log unit neutral density filter. Receptive fields (RFs) of GCs were mapped using white noise binary checkerboards, and the spike triggered average (STA) of a GC will be calculated for each pixel in the 32×32 2-D array [27,28]. The spatial profiles of STAs will be fitted by 2-D Gaussian functions, and GC RFs are represented by nine 1-s.d. annulus contours [29]. The RF center STA is calculated as the weighted average of the mean STAs of the three center annuli, and the RF surround as the weighted average of the mean STAs of annuli 4–9 [25]. RF size of a GC is represented as mean radius (square root of the product of major and minor radii of an elliptic contour). Whole-field light stimulation was carried out by a light pipe (with 9 log unit neutral density filters to be compatible with the WVC stimulator) [30].

2.7. Statistical tests

Statistical tests and significance values are indicated in the text and figure legends. For comparison of populations we used the Student’s t-test when normally distributed, otherwise we used a Kolmogorov-Smirnov (KS) test or a Wilcoxon signed-rank test (Mann-Whitney U test) [31,32]. In all cases we applied a Bonferroni correction to account for multiple comparisons.

3. Results

3.1. The percentage of retinal ganglion cells with responsive scotopic and photopic spike triggered averages (STA) varied in wild-type (WT), Bhlhb4$^{-/-}$, Tra$^{-/-}$, Gnat2^{cpfl3} and Cx36$^{-/-}$ mice.

In order to study synaptic pathways mediating spatiotemporal responses of mammalian GCs, we employed reverse correlation methods to obtain spike triggered averages (STAs) of GCs recorded with the MEA in *WT (C57/B6J)*, *Bhlhb4*$^{-/-}$, *Tra*$^{-/-}$, *Gnat2*^{cpfl3} and *Cx36*$^{-/-}$ mice in response to the white-noise checkerboard stimulation [25]. A STA was considered responsive if any of its values was greater than five times the standard deviation of every value of the STA. We obtained STAs under both scotopic and photopic conditions (a −3 log unit neutral density filter was added to the LED for scotopic stimulation, [25]. Figure 2 shows the percentage of GCs with responsive STAs by mouse strain and lighting condition, with numbers of cells given in columns 2 and 3 of Table 1. In 15 wild-type retinas with a total of 342 GCs, we found 191 GCs (56%) had responsive STAs in photopic conditions, and 78 (23%) had responsive STAs in scotopic conditions. In 8 *Gnat2*^{cpfl3} retinas (310 GCs), we found a general decrease in responsivity, only 44 GCs (14%) had photopic STAs and 18 GCs (5.6%) had scotopic STAs. In *Tra*$^{-/-}$ and *Bhlhb4*$^{-/-}$ retinas we saw a more drastic decline in scotopic responses. In 9 *Bhlhb4*$^{-/-}$ retinas (272 GCs) we had 83 photopic STAs (31%) but only 5 scotopic STAs (1.9%), and in 6 *Tra*$^{-/-}$ retinas (232 GCs), we found 107 cells with responsive photopic STAs (46%) and 0 cells with responsive scotopic STAs. In 7 *Cx36*$^{-/-}$ retinas (221GCs), we had 97 (39%) photopic STAs and 31 (14%) scotopic STAs.

3.2. GC scotopic and photopic temporal processing in WT, Bhlhb4$^{-/-}$, Tra$^{-/-}$, Gnat2^{cpfl3} and Cx36$^{-/-}$ mice

We examined the temporal processing within the receptive field center of GCs. To define a GC's receptive field center, we fit a two-dimensional Gaussian function to the peak temporal slice of its STA [25]. The receptive field center was defined as the area within the first three standard deviations of this spatial Gaussian [24]. To look at temporal processing in the center, we computed a weighted average of the temporal filters falling within it, combining them into a single temporal filter. We then sorted the STAs into two categories: linear ON and linear OFF (L-ON and L-OFF) based on the polarity of the STA's peak temporal response. By convention, STAs of L-ON GCs have positive polarity (light on is represented by +1) and STAs of L-OFF GCs have negative polarity (light off is represented by −1) [33]. We found that all sustained ON GCs and transient ON GCs exhibit L-ON STAs and all sustained OFF, transient OFF and ON-OFF GCs exhibit L-OFF STAs, consistent with the results in our previous publication [33]. The numbers of responsive L-ON GCs and L-OFF GCs in our responsive GC pool are given in columns 4 and 5 of Table 1.

The mean receptive field center STAs of L-ON GCs and L-OFF GCs in *WT*, *Bhlhb4*$^{-/-}$, *Gnat2*^{cpfl3} and *Cx36*−/− mice under scotopic conditions are shown as thick traces (averaged over numbers of GCs listed in columns 4 and 5 of Table 1, shaded area represents +/− two standard errors) in Figure 3Aa and 3Ab respectively. To quantify differences in temporal processing, we considered two parameters for each GC's center temporal filter. The first was time-to-peak (TTP), the amount of time between the peak of the STA and the spike time (see

insert of Figure 3). This measures the latency between stimulation and the GC peak response, and longer/shorter TTP tunes GC responses to lower/higher frequencies. The second parameter was biphasic index (BI), which compares the size of the second peak of the center STA to that of the first peak in order to quantify how biphasic a temporal filter is (see insert of Figure 3). The first peak reflects BC inputs and the second peak reflects inputs of antagonistic polarity mediated by polysynaptic circuit involving narrow-field HCs or ACs [24], and therefore BI represents the *ratio of antagonistic to center synaptic inputs*. Figure 3Acd are mean TTPs (averaged over numbers of L-ON and L-OFF GCs given in Table 1 columns 4 and 5, error bars are standard errors) under scotopic conditions. The average TTP of ON GCs in *WT*, *Bhlhb4*$^{-/-}$, *Gnat2*^{cpfl3} and *Cx36*$^{-/-}$ mice are 0.23, 0.23, 0.23 and 0.17 sec, respectively; and the average TTP of OFF GCs in *WT*, *Gnat2*^{cpfl3} and *Cx36*$^{-/-}$ mice are 0.28, 0.28 and 0.23 sec, respectively. The TTPs of ON GC STAs in *Cx36*$^{-/-}$ mice were shorter than that of the WT mice whereas those in the *Bhlhb4*$^{-/-}$and *Gnat2*^{cpfl3} mice showed no significant difference. The TTP of OFF GC STAs in *Cx36*$^{-/-}$ mice were also shorter than that of the WT mice whereas those in the *Gnat2*^{cpfl3} mice were not significant altered. The average BI (and SE bars) shown in Figure 3Ae of ON GCs in *WT*, *Bhlhb4*$^{-/-}$, *Gnat2*^{cpfl3} and *Cx36*$^{-/-}$ mice are 0.33, 0.30, 0.03 and 0.04, respectively; and the average BI of OFF GCs in *WT*, *Gnat2*^{cpfl3} and *Cx36*$^{-/-}$ mice shown in Figure 3Af are 0.3, 0.4 and 0.2, respectively. The BIs of ON GC STA in *Gnat2*^{cpfl3} and *Cx36*$^{-/-}$ mice were much smaller than that in the WT mice whereas those in the *Bhlhb4*$^{-/-}$ mice did not significantly differ (though the second peak was shorter, Figure 3A magenta trace). The BIs of OFF GC STA in *Gnat2*^{cpfl3} are significantly larger and in *Cx36*$^{-/-}$ mice were smaller than that in the WT mice. For comparison between parameters from various mouse strains and between parameters measured under scotopic and photopic conditions, these mean TTP and BI values are listed in Table 2 columns 4 and 6. The values of mutant mice higher than the corresponding values in WT mice are in red, and those lower than the WT values are in blue in Table 2.

Figures 3Ba and 3Bb are the mean STA traces of L-ON and L-OFF GCs of the WT and four mutant mouse lines in photopic conditions (thick traces, averaged over numbers of GCs listed in columns 4 and 5 of Table 1, shaded area represents +/− two standard errors). Figure 3Bcd are the mean TTPs (averaged over same numbers of cells, error bars are standard errors) for ON and OFF GCs in the WT and four mutant mouse lines under photopic conditions. The TTPs are generally shorter in all mice as compared with the corresponding values in scotopic conditions. The mean TTP of ON GCs in *WT*, *Bhlhb4*$^{-/-}$, *Tra*$^{-/-}$, *Gnat2*^{cpfl3} and *Cx36*$^{-/-}$ mice are 0.12, 0.15, 0.12, 0.15 and 0.135 sec, respectively; and the mean TTP of OFF GCs are 0.13, 0.12, 0.12, 0.16 and 0.12 sec, respectively. ON GC STAs in *Bhlhb4*$^{-/-}$ mice had longer TTPs than wild type, as did ON GCs in *Gnat2*^{cpfl3} and Cx36−/− mice, while TTPs in *Tra*$^{-/-}$ mice were unchanged. In OFF cells, STA from *Gnat2*^{cpfl3} mice had a longer TTP, while those from *Bhlhb4*$^{-/-}$, *Tra*$^{-/-}$ and *Cx36*−/− mice showed no significant difference in TTP. The average BI of ON GCs in *WT*, *Bhlhb4*$^{-/-}$, *Tra*$^{-/-}$, *Gnat2*^{cpfl3} and *Cx36*$^{-/-}$ mice are 0.24; 0.16; 0.26; 0.27 and 0.36, respectively; and the average BI of OFF GCs are 0.22 0.36, 0.18, 0.25 and 0.33, respectively (Figure 3Bef). Among ON cells, *Bhlhb4*$^{-/-}$ mice were significantly less biphasic. In OFF cells, those from *Bhlhb4*$^{-/-}$ mice were significantly more biphasic, as were those from *Gnat2*^{cpfl3} and

Cx36$^{-/-}$ mice, but those from *Tra*$^{-/-}$ mice were slightly less biphasic. The mean TTP and BI values obtained under photopic conditions are also listed in Table 2 columns 5 and 7.

As shown in this and section (3.1), nearly all GCs in *Bhlhb4*$^{-/-}$ and *Tra*$^{-/-}$mice do not have responsive STAs in scotopic conditions (Tables 1 and 2). Therefore in the following sections where we compare spatial response properties of GCs in the WT and four mutant mouse lines, we focus on GCs recorded under *photopic* conditions.

3.3. GC Receptive Field Center Size in WT, Bhlhb4$^{-/-}$, Tra$^{-/-}$, Gnat2^{cpfl3} and Cx36−/− mice under photopic conditions

We next looked at the receptive field center size of GCs in the four types of mutant mice to determine how rod and cone pathways affect the spatial structure of the GC receptive fields (RFs). Using the Gaussian fits described in the previous section, we computed the RF center radius (square root of the product of major and minor radii of the elliptic contour of a GC's RF center (Figure 4 insert 1) of each GC. Figure 4A shows the distribution of mean *photopic* receptive field center radii of ON GCs (Aa, *WT*, *Bhlhb4*$^{-/-}$, *Tra*$^{-/-}$, *Gnat2*^{cpfl3} *and Cx36*−/− mice: 70.8, 58.8*, 67.8, 66.5 and 59.0*, error bars = S.E.) and OFF GCs (Ab, 74.3, 71.5, 77.8, 72.4 and 59.8, error bars = S.E.) in the five mouse strains. The mean RF center radius values are also listed in Table 2 column 8. The RF center radius of ON cells from *Bhlhb4*$^{-/-}$ mice were significantly smaller than those of wild-type mice, while the RF center radius of OFF *Bhlhb4*$^{-/-}$ cells was not significantly different. The RF center radius of both ON and OFF cells from *Cx36*$^{-/-}$ mice were significantly smaller than those of wild-type mice. There was no significant difference in RF center size for either ON or OFF cells in *Tra*$^{-/-}$ or *Gnat2*^{cpfl3} mice.

Thus, removing rod bipolar cells reduces the receptive field size of ON GCs. The fact that removing bipolar cells, but not photoreceptors, leads to a change in center size suggests that bipolar cells may be the key cells in determining the size of GC receptive field centers. Moreover, suppressing rod-cone coupling (secondary cone pathway), AIIAC-BC coupling (tertiary cone pathway) and GC-GC coupling (pathway 4) reduces RF center size of both ON and OFF GCs.

3.4. Strength of GC antagonistic surround responses in WT, Bhlhb4$^{-/-}$, Tra$^{-/-}$, Gnat2^{cpfl3} and Cx36$^{-/-}$ mice under photopic conditions

A hallmark of spatial processing in retinal ganglion cells is the presence of center-surround antagonism: light falling on a cell's RF surround elicits responses of the opposite polarity as light on the RF center [25,33]. Previous work from our lab has shown that WT mouse GCs have a linear antagonistic surround under photopic conditions [25], so we sought to determine if it is altered by various combinations of pathway suppression in mutant mice.

To quantify the presence and polarity of the surround, we first combined inputs from the outer portions (from 4 s.d. to 9 s.d. of the Gaussian fit) of the receptive field into a single temporal trace, in a similar fashion as we did the center. We compared the strength and polarity of the surround to that of the center using a measure called the surround polarity index (SPI). The SPI is computed by dividing each cell's STA into center and surround regions, combined all inputs within each region into a single trace, then integrated the area

under each trace from the time of the spike to the peak of the STAs, and took the ratio of the integrals of the surround to that of the center as the SPI (Figure 4 insert 2). The absolute value of the SPI indicates the surround's strength relative to the center, and its sign indicates whether the surround is antagonistic (SPI < 0) or synergistic (SPI > 0) [33].

The average SPI of ON and OFF GCs from the WT and four mutant mouse lines are shown in Figure 4B, and they are also listed in Table 2 column 9. We found that *Cx36*$^{-/-}$ ON and OFF GCs and *Gnat2*^{cpfl3} OFF cells showed statistically significant SPI increases (decreases of antagonistic surround). On the other hand, no significant SPI change was observed in *Bhlhb4*$^{-/-}$ or *Tra*$^{-/-}$ GCs. These results indicate that gap junctions in the secondary and tertiary cone pathways are involved in mediating antagonistic surround of ON GCs, and cones are responsible for most if not all the antagonistic surround response in OFF RGCs.

4. Discussion

4.1. Contributions of various rod and cone pathways to GC responsiveness in scotopic and photopic conditions

In this study, we investigated scotopic and photopic spatiotemporal response profiles of retinal ganglion cells (GCs) in wild-type (WT) and four pathway-specific mutant mouse lines. Results from previous studies have shown that the *Bhlhb4*$^{-/-}$ mouse lacks rod-bipolar cells [23]; the *Tra*$^{-/-}$ mouse lacks rod signals [21]; the *Gnat2*^{cplf3} mouse lacks cone signals [22]; and the *Cx36*$^{-/-}$ mouse lacks rod-cone coupling, AIIAC coupling and some GC-GC coupling [10,14,20]. Consequently, as marked by "X"s in Figure 1, the primary rod pathway, the secondary and tertiary cone pathways are suppressed in the *Bhlhb4*−/− mouse; all three rod pathways are suppressed in the *Tra*$^{-/-}$ mouse; all three cone pathways are suppressed in the *Gnat2*^{cpfl3} mice; and the primary rod pathway and the tertiary cone pathway for ON GCs are suppressed and the secondary rod pathway, the secondary cone pathway and pathway 4 are suppressed in both ON and OFF GCs in the *Cx36*$^{-/-}$ mouse. These pathway suppressions in the four mutant mouse lines are listed in column 1 of Table 2 (R1, R2, R3, C1, C2 and C3 are primary, secondary and tertiary rod or cone pathways). By comparing the percentage of GCs with responsive scotopic and photopic STAs in WT mouse and the four mutant mouse lines, we sought to determine contributions of various rod and cone pathways to spatiotemporal response profiles of GCs under scotopic and photopic conditions.

In general, there is a lower percentage of GCs with responsive scotopic and photopic STAs in all four strains of mutant mice as compared with the percentage of responsive GCs in WT mice (Figure 2), consistent with the idea that suppression of any set of rod and cone pathways reduces the responsiveness of GCs.

Under scotopic conditions, no GCs in *Tr*a−/− mice and very few OFF GCs in *Bhlhb4*−/− mice had responsive STAs, indicating that GC light responses in scotopic conditions require rod pathways (R1–3), especially the primary rod pathway (rod BCs, R1) [23]. This means GCs in *Tr*a−/− mice did not encode spatiotemporal information in dim light, which is consistent with the flash ERG data showing that these mice lack scotopic b-wave [19,21] and with data showing the *Tr*a−/− mice lack optokinetic reflexes in scotopic light [30]. The small group of responsive OFF GCs in the *Bhlhb4*−/− mice (no primary rod pathway or no

R1) suggests that secondary and tertiary rod pathways (R2 and R3) are responsible for mediating scotopic vision in some OFF GCs [19,30,34], consistent with the scotopic optokinetic reflexes data [30]. A substantial percentage of GCs exhibit responsive scotopic STAs in *Cx36*$^{-/-}$ mice (no R1 for ON GCs, no R2), suggesting that the tertiary rod pathways (R3) play a significant role in mediating scotopic vision in subpopulations of GCs.

Under photopic conditions, the percentage of GCs with responsive STA in the *Tr*a−/− mice is about 18% lower than that in the WT mice, suggesting that rods play a significant but minor role in photopic vision. However, a significant number of photopic STAs is found in GCs from *Gnat2*^{cpfl3} mice (14% as compared with 56% in WT mice), suggesting that rods play a significant role in photopic responses of some GCs. The *Cx36*$^{-/-}$ data suggest that with suppression of rod-cone coupling (secondary rod pathway, R2) and AIIAC-ON cone BC coupling (tertiary cone pathway, R3), the tertiary cone pathway (C3) plays a significant role in photopic responses of GCs.

By comparing the percentage of GCs with responsive STAs in scotopic conditions and in photopic conditions of the same mouse strain (columns 2 and 3 of Table 2), we sought to investigate adaptation-induced changes in GC responsiveness in each mouse strain. It is evident in all five mouse strains that light adaptation increases the number of responsive GCs, suggesting that cone pathways are able to generate light responses in more GCs than rod pathways. This assertion is supported by our observation that the least difference between responsive photopic and scotopic GCs was found in retinas without cone inputs (*Gnat2*^{cpfl3}, 14%−5.8%=8.2%) whereas the largest difference was in retinas without rod inputs (*Tr*a$^{-/-}$, 46%−0%=46%). Although mouse is a nocturnal animal, our data suggest their retinal ganglion cells are more active in photopic or mesopic conditions.

4.2. Contributions of rod and cone pathways to temporal processing of mouse GC responses in scotopic and photopic conditions.

We also found differences in the temporal processing between mutant and WT mice. Under scotopic conditions, ON and OFF GCs in *Cx36*$^{-/-}$ mice had shorter average TTP and were less biphasic, suggesting that gap junctions in primary and secondary rod pathways slow down GCs' scotopic light responses and increase the ratio of inputs of antagonistic polarity (mediated by polysynaptic circuits comprised of narrow field horizontal cells or narrow-field amacrine cells) to BC inputs of center polarity [25]. Comparing with WT mice, scotopic STAs in *Gnat2*^{cpfl3} mice had similar average TTP, but different BI. This suggests cone pathways do not affect the kinetics of scotopic GC responses but alter the ratio of BC and narrow-field AC/HC inputs.

Under photopic conditions, ON GCs in *Bhlhb4*$^{-/-}$, *Gnat2*^{cpfl3} and *Cx36*$^{-/-}$ mice, as well as OFF GCs in *Gnat2*^{cpfl3} mice had longer TTPs, suggesting that various combinations of cone pathways speed up GCs photopic light responses. BI of ON GCs in *Bhlhb4*$^{-/-}$ and *Cx36*−/− mice, as well as BI of OFFGCs in *Bhlhb4*$^{-/-}$, *Tra*$^{-/-}$, *Gnat2*^{cpfl3} and *Cx36*$^{-/-}$ mice are different compared with the WT mice. This suggests that various combinations of cone pathways (C1–3) alters the ratio of BCs and narrow-field AC/HC inputs. We found that knocking out rod bipolar cells had asymmetric effects on spatiotemporal processing in ON and OFF RGCs. ON cells in *Bhlhb4*$^{-/-}$ mice had a longer TTP and smaller BI, suggesting

that rod bipolar cells shorten the response latency of ON GCs and tune ON GC photopic responses to higher frequencies. In contrast, OFF cells only had an increased BI, suggesting rod bipolar cells play a role in tuning OFF RGC photopic responses to lower frequencies.

In addition to the TTP and BI differences between mutant and WT mice, there are significant differences in TTP and BI values measured between scotopic and photopic conditions (compare columns 4 and 5, and compare columns 6 and 7 of Table 2). In *WT*, *Gnat2*^{cpfl3} and *Cx36*−/− mice (*Bhlhb4*$^{-/-}$ and *Tra*$^{-/-}$mice had insufficient number of responsive GCs in scotopic conditions), adapting to brighter ambient light (light adaptation) shortens TTP of both ON and OFF GCs by 18–54%, in effect speeding up GCs' temporal processing and tuning GC photopic responses to higher frequencies. Our observation that suppression of cone signals (C1–3) in *Gnat2*^{cpfl3} mice or connexin36 gap junction channels (R1–2+C2–3+4) in *Cx36*−/− mice preserves the response speedup suggests that the tertiary rod pathway plays a significant role in the adaptation-induced TTP changes in some WT GCs.

Light adaptation makes GC responses in WT mice less biphasic, but GCs in *Gnat2*^{cpfl3} and *Cx36*−/− mice more biphasic. This suggests that the cone pathways (suppressed in *Gnat2*^{cpfl3} mice) and Cx36 gap junction channels (suppressed in *Cx36*−/− mice) are responsible for the adaptation-induced reduction of antagonistic inputs to GCs in the WT mice.

4.3. Effects of rod/cone pathway suppression on GCs' receptive field profiles in photopic conditions

Our results show that the receptive field center (RFC) size of ON GCs in *Bhlhb4*$^{-/-}$ and *Cx36*$^{-/-}$ mice and of OFF GCs in *Cx36*$^{-/-}$ mice were smaller as compared with the WT mice. Since AII amacrine cell (AIIAC) responses in both *Bhlhb4*$^{-/-}$ and *Cx36*$^{-/-}$ mice are reduced [14], we attribute the GC RFC size reduction partially to the decrease of AIIAC response and RF (caused by no rod BC inputs in *Bhlhb4*$^{-/-}$ and AII-AII-cone ON BC uncoupling in *Cx36*$^{-/-}$), as GC RFCs are partially mediated by inputs from AIIACs [35]. AIIACs send signals to ON GCs through gap junctions to cone ON BCs [36] and to OFF GCs via glycinergic synapses to OFF BC and OFF GCs [37,38]. RFC reduction is observed only in ON GCs in the *Bhlhb4*$^{-/-}$ mice but in both ON and OFF GCs in *Cx36*$^{-/-}$ mice because decrease of AIIAC response and RF under scotopic conditions in the *Bhlhb4*$^{-/-}$ mice (primary rod pathway suppression) is weaker. We also attribute RFC size decrease of ON and OFF GCs in *Cx36*$^{-/-}$ mice to uncoupling of gap junctions between GCs (pathway 4 in Figure 1), as it has been shown that connexin36 mediates coupling of alpha ganglion cells in the mouse retina [20].

In addition to RFC sizes, we found that the surround polarity index (SPI) of ON GCs in *Cx36*$^{-/-}$ mice and that of the OFF GCs in *Gnat2*^{cpfl3} mice under photopic conditions were less negative (weaker antagonistic surround responses). Since antagonistic surround responses of GCs are largely mediated by wide-field ACs and HCs [39], our results suggest that connexin36 gap junctions and cone pathways are involved in synaptic circuits (wide-field AC/HCs) underlying surround inputs to GCs. On the other hand, SPI of ON and OFF

GCs in *Bhlhb4*$^{-/-}$ mice did not change, meaning that the rod bipolar cells play a minor role in mediating antagonistic surround responses of GCs.

4.4. Summary of rod and cone pathway contributions to GC response kinetics and receptive field profile in scotopic and photopic conditions

Based on our analysis of GC spatiotemporal responses in WT and four pathway-specific knockout mouse strains discussed above, contributions of various rod and cone pathways (R1–3, C1–3) and GC coupling (pathway 4) to response kinetics and receptive field profiles of ON and OFF GCs under scotopic and photopic conditions are summarized below.

Scotopic responses of some GCs require all three rod pathways (R1–3), some require only the secondary and tertiary rod pathways (R2–3), and others require only the tertiary rod pathway (R3). There are more responsive GCs in photopic conditions mediated by cone pathways (C1–3) than responsive GCs in scotopic conditions generated by rod pathways (R1–3). Gap junctions slow down GCs' scotopic light responses and tune responses to lower frequencies, they also increase the ratio of GCs' antagonistic to center synaptic inputs. Cone pathways (C1–3) do not affect the kinetics but alter the GCs' antagonistic to center synaptic inputs of scotopic GC responses. They also speed up GCs photopic responses and alter the ratio of GCs' antagonistic to center synaptic inputs and receptive field profiles. Rod bipolar cells shorten response latencies of ON GCs and tune ON GC photopic responses to higher frequencies, and they increase the ratio of GCs' antagonistic to center synaptic inputs. Light adaptation speeds up GCs' temporal processing and tunes GC photopic responses to higher frequencies, and the tertiary rod pathway (R3) plays a significant role in such adaptation-induced TTP changes in some WT GCs. GC RF center sizes are partially mediated by AIIACs and GC-GC coupling (pathway 4). Connexin36 gap junctions and cone pathways (C1–3) alter synaptic circuits underlying antagonistic surround inputs to GCs in photopic conditions.

Acknowledgements

We thank Roy Jacoby for critically reading this manuscript. This work was supported by grants from NIH (EY019908), NIH Vision Core (EY 02520), the Retina Research Foundation (Houston), and the Research to Prevent Blindness, Inc.

Abbreviations:

GC	retinal ganglion cell
BC	bipolar cell
AC	amacrine cell
AIIAC	AII amacrine cell
Trα	rod transducin
Gnat2^{cplf3}	guanine nucleotide binding protein alpha transducing activity polypeptide 2 (cone transducin mutant)

Cx36	connexin36
Bhlhb4	basic helix-loop-helix beta 4
R1, R2 and R3	primary, secondary and tertiary rod pathway
C1, C2 and C3	primary, secondary and tertiary cone pathway

Reference List

1. Dowling JE. The Retina, an approachable part of the brain. Revised edition ed. Harvard University Press; 2012.
2. Masland RH. The fundamental plan of the retina. Nat.Neurosci 2001 9;4(9):877–86 [PubMed: 11528418]
3. Volgyi B, Chheda S, Bloomfield SA. Tracer coupling patterns of the ganglion cell subtypes in the mouse retina. J Comp Neurol. 2009 2 10;512(5):664–87 [PubMed: 19051243]
4. Boycott B, Wassle H. Parallel processing in the mammalian retina: the Proctor Lecture. Invest Ophthalmol.Vis.Sci 1999 6;40(7):1313–27 [PubMed: 10359312]
5. Kolb H The architecture of functional neural circuits in the vertebrate retina. The Proctor Lecture. Invest Ophthalmol.Vis.Sci 1994 4;35(5):2385–404 [PubMed: 8163331]
6. Pang JJ, Gao F, Lem J, Bramblett DE, Paul DL, Wu SM. Direct rod input to cone BCs and direct cone input to rod BCs challenge the traditional view of mammalian BC circuitry. Proc.Natl.Acad.Sci.U.S.A 2010 1 5;107(1):395–400 [PubMed: 20018684]
7. Pang JJ, Gao F, Paul DL, Wu SM. Rod, M-cone and M/S-cone inputs to hyperpolarizing bipolar cells in the mouse retina. J.Physiol 2012 2 15;590(Pt 4):845–54 [PubMed: 22219344]
8. Tsukamoto Y, Morigiwa K, Ishii M, Takao M, Iwatsuki K, Nakanishi S, Fukuda Y. A novel connection between rods and ON cone bipolar cells revealed by ectopic metabotropic glutamate receptor 7 (mGluR7) in mGluR6-deficient mouse retinas. J.Neurosci 2007 6 6;27(23):6261–7 [PubMed: 17553999]
9. Tsukamoto Y, Morigiwa K, Ueda M, Sterling P. Microcircuits for night vision in mouse retina. J.Neurosci 2001 11 1;21(21):8616–23 [PubMed: 11606649]
10. Deans MR, Volgyi B, Goodenough DA, Bloomfield SA, Paul DL. Connexin36 is essential for transmission of rod-mediated visual signals in the mammalian retina. Neuron 2002 11 14;36(4):703–12 [PubMed: 12441058]
11. Ribelayga C, Cao Y, Mangel SC. The circadian clock in the retina controls rod-cone coupling. Neuron 2008 9 11;59(5):790–801 [PubMed: 18786362]
12. Zhang J, Wu SM. Connexin35/36 gap junction proteins are expressed in photoreceptors of the tiger salamander retina. J.Comp Neurol 2004;470:1–12 [PubMed: 14755521]
13. Li W, Devries SH. Separate blue and green cone networks in the mammalian retina. Nat.Neurosci 2004 7;7(7):751–6 [PubMed: 15208635]
14. Pang JJ, bd-El-Barr MM, Gao F, Bramblett DE, Paul DL, Wu SM. Relative contributions of rod and cone bipolar cell inputs to AII amacrine cell light responses in the mouse retina. J.Physiol 2007 4 15;580(Pt. 2):397–410 [PubMed: 17255172]
15. Trexler EB, Li W, Mills SL, Massey SC. Coupling from AII amacrine cells to ON cone bipolar cells is bidirectional. J.Comp Neurol 2001 9 3;437(4):408–22 [PubMed: 11503143]
16. Pang JJ, Gao F, Wu SM. Light-evoked excitatory and inhibitory synaptic inputs to ON and OFF alpha ganglion cells in the mouse retina. J.Neurosci 2003 7 9;23(14):6063–73 [PubMed: 12853425]
17. Arman AC, Sampath AP. Dark-adapted response threshold of OFF ganglion cells is not set by OFF bipolar cells in the mouse retina. J.Neurophysiol 2012 5;107(10):2649–59 [PubMed: 22338022]
18. Chun MH, Han SH, Chung JW, Wassle H. Electron microscopic analysis of the rod pathway of the rat retina. J.Comp Neurol 1993 6 22;332(4):421–32 [PubMed: 8349841]

19. Abd-El-Barr MM, Pennesi ME, Saszik SM, Barrow AJ, Lem J, Bramblett DE, Paul DL, Frishman LJ, Wu SM. Genetic Dissection of Rod and Cone Pathways in the Dark-adapted Mouse Retina. J.Neurophysiol 2009 7 8;102:1945–55 [PubMed: 19587322]
20. Schubert T, Degen J, Willecke K, Hormuzdi SG, Monyer H, Weiler R. Connexin36 mediates gap junctional coupling of alpha-ganglion cells in mouse retina. J.Comp Neurol 2005 5 9;485(3):191–201 [PubMed: 15791644]
21. Calvert PD, Krasnoperova NV, Lyubarsky AL, Isayama T, Nicolo M, Kosaras B, Wong G, Gannon KS, Margolskee RF, Sidman RL, et al. Phototransduction in transgenic mice after targeted deletion of the rod transducin alpha -subunit. Proc.Natl.Acad.Sci.U.S.A 2000 12 5;97(25):13913–8 [PubMed: 11095744]
22. Chang B, Dacey MS, Hawes NL, Hitchcock PF, Milam AH, tmaca-Sonmez P, Nusinowitz S, Heckenlively JR. Cone photoreceptor function loss-3, a novel mouse model of achromatopsia due to a mutation in Gnat2. Invest Ophthalmol.Vis.Sci 2006 11;47(11):5017–21 [PubMed: 17065522]
23. Bramblett DE, Pennesi ME, Wu SM, Tsai MJ. The transcription factor Bhlhb4 is required for rod bipolar cell maturation. Neuron 2004;43 :779–93 [PubMed: 15363390]
24. Cowan CS, Sabharwal J, Seilheimer RL, Wu SM. Distinct subcomponents of mouse retinal ganglion cell receptive fields are differentially altered by light adaptation. Vision Res. 2017 1 10;
25. Cowan CS, Sabharwal J, Wu SM. Space-time codependence of retinal ganglion cells can be explained by novel and separable components of their receptive fields. Physiol Rep. 2016 9;4(17)
26. Pang JJ, Gao F, Wu SM. Light-evoked current responses in rod bipolar cells, cone depolarizing bipolar cells and AII amacrine cells in dark-adapted mouse retina. J.Physiol 2004;559(1):123–35
27. Chichilnisky EJ. A simple white noise analysis of neuronal light responses. Network. 2001 5;12(2):199–213 [PubMed: 11405422]
28. Meister M, Pine J, Baylor DA. Multi-neuronal signals from the retina: acquisition and analysis. J.Neurosci.Methods 1994 1;51(1):95–106 [PubMed: 8189755]
29. Field GD, Greschner M, Gauthier JL, Rangel C, Shlens J, Sher A, Marshak DW, Litke AM, Chichilnisky EJ. High-sensitivity rod photoreceptor input to the blue-yellow color opponent pathway in macaque retina. Nat.Neurosci 2009 9;12(9):1159–64 [PubMed: 19668201]
30. Cowan CS, Abd-El-Barr M, van der Heijden M, Lo EM, Paul D, Bramblett DE, Lem J, Simons DL, Wu SM. Connexin 36 and rod bipolar cell independent rod pathways drive retinal ganglion cells and optokinetic reflexes. Vision Res. 2016 2;119:99–109. [PubMed: 26718442]
31. Marmarelis PZ, Naka K. Experimental analysis of a neural system: two modeling approaches. Kybernetik. 1974 5 31;15(1):11–26 [PubMed: 4851971]
32. Godfrey MG, Roebuck EM, Sherlock AJ. Concise Statistics. London: Edward Arnold Ltd 1988.
33. Sabharwal J, Seilheimer RL, Tao X, Cowan CS, Frankfort BJ, Wu SM. Elevated IOP alters the space-time profiles in the center and surround of both ON and OFF RGCs in mouse. Proc.Natl.Acad.Sci.U.S.A 2017 8 15;114(33):8859–64. [PubMed: 28760976]
34. Sabharwal J, Seilheimer RL, Cowan CS, Wu SM. The ON Crossover Circuitry Shapes Spatiotemporal Profile in the Center and Surround of Mouse OFF Retinal Ganglion Cells. Front Neural Circuits. 2016;10:106. [PubMed: 28066192]
35. Bloomfield SA, Dacheux RF. Rod vision: pathways and processing in the mammalian retina. Prog.Retin.Eye Res 2001 5;20(3):351–84 [PubMed: 11286897]
36. Kolb H, Famiglietti EV. Rod and cone pathways in the inner plexiform layer of cat retina. Science 1974 10 4;186(4158):47–9 [PubMed: 4417736]
37. Kolb H, Famiglietti EV. Rod and cone pathways in the inner plexiform layer of cat retina. Science. 1974 10 4;186(4158):47–9 [PubMed: 4417736]
38. Bolz J, Wassle H, Thier P. Pharmacological modulation of on and off ganglion cells in the cat retina. Neuroscience. 1984 7;12(3):875–85 [PubMed: 6147791]
39. Werblin FS, Dowling JE. Organization of the retina of the mudpuppy, Necturus maculosus. II. Intracellular recording. J.Neurophysiol 1969 5;32(3):339–55 [PubMed: 4306897]

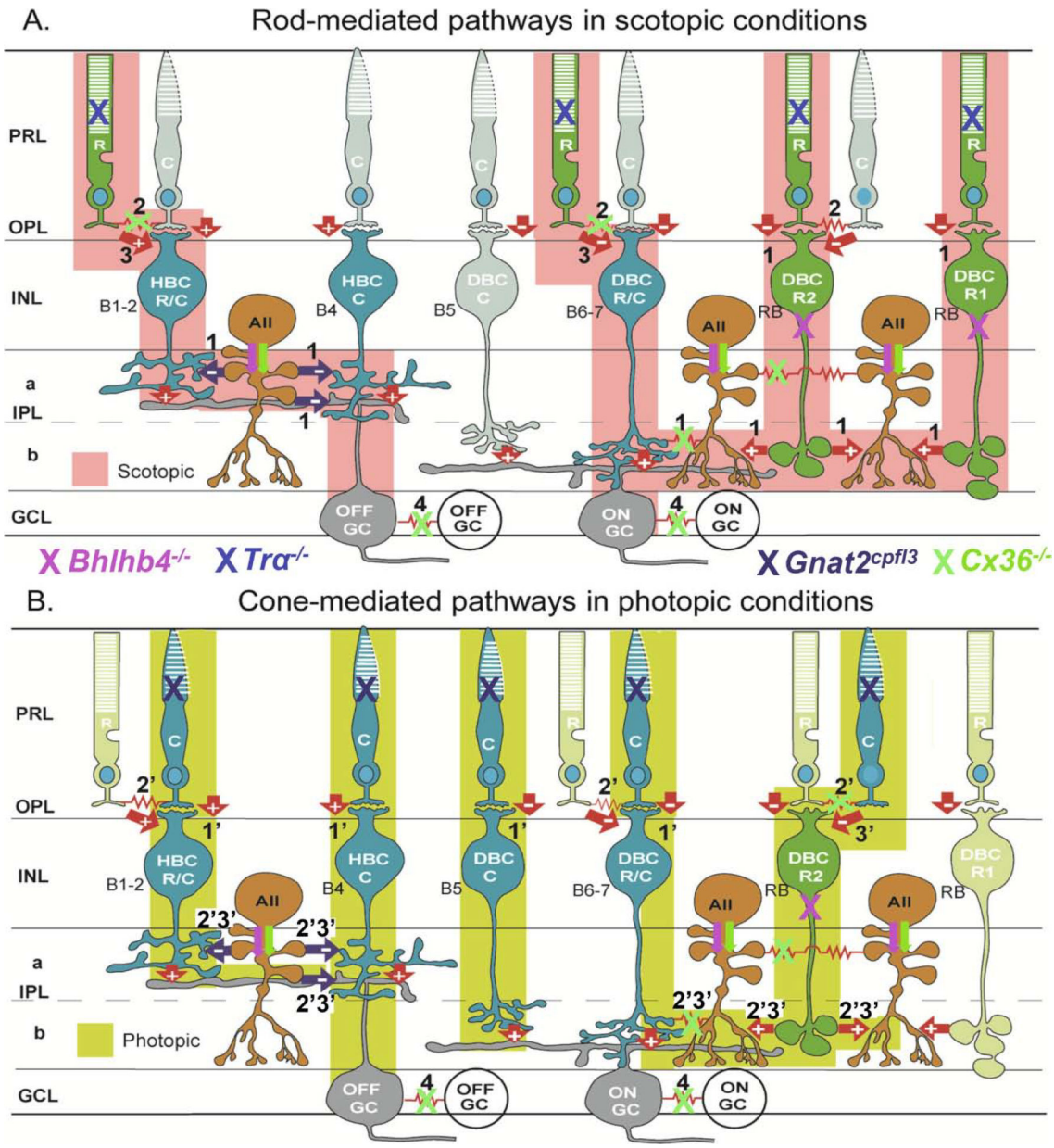

Figure 1. Schematic diagram of major synaptic pathways mediating light responses of mouse ON and OFF ganglion cells in scotopic (A) and photopic (B) conditions.

R: rod, C: cone, $HBC_{R/MC}$: Mixed rod/M-cone hyperpolarizing bipolar cell; HBC_{MC}: M-cone hyperpolarizing bipolar cell; DBC_{MC}: M-cone depolarizing bipolar cell, $DBC_{R/MC}$: Mixed rod/M-cone depolarizing bipolar cell; DBC_{R2}: type 2 rod depolarizing bipolar cell; DBC_{R1}: type 1 rod depolarizing bipolar cell; AII: AII amacrine cell; OFFGC: OFF ganglion cell; ONGC: ON ganglion cell; green: rods and rod BCs; blue: cones and cone BCs, dark orange: ACs; grey: GCs; arrows: chemical synapses (red: glutamatergic, black: glycinergic, "+" sign-preserving, and "−"sign-inverting), red zigzag: electrical synapses (Cx36), PRL: photoreceptor layer, OPL: outer plexiform layer, INL: inner nuclear layer, IPL: inner plexiform layer (a: sublamina a, b: sublamina b), GCL: ganglion cell layer. Tentative correlations between anatomical BC types (B1–7 and RB, in black letters) and physiological

BC types are given. Rod pathways that operate in scotopic conditions are colored pink and marked 1–3: (1) rod-DBC_R-AII-DBC_C/HBC_C-ONGC/OFFGC, (2) rod↔cone→DBC_C/HBC_C-ONGC/OFFGC and (3) rod-DBC_C/HBC_C-ONGC/OFFGC. Cone pathways that operate in photopic conditions are colored yellow and marked 1'−3': (1') cone-DBC_C/HBC_C - ONGC/OFFGC, (2') cone-rod-DBC_R-AII-DBC_C /HBC_C-ONGC/OFFGC, and (3') cone-DBC_R-AII - DBC_C/HBC_C-ONGC/OFFGC. GC-GC couplings are marked as 4. Active cells are marked with full colors and inactive cells are with unsaturated colors. Pathway suppressions in *Bhlhb4*$^{-/-}$, *Tra*$^{-/-}$, *Gnat2*^{cpfl3} and *Cx36*$^{-/-}$ mice are marked by pink, blue, black and green "X"s, respectively. Pink and green arrows indicate decreased AIIAC responses in the in *Bhlhb4*$^{-/-}$ and *Cx36*$^{-/-}$ mice.

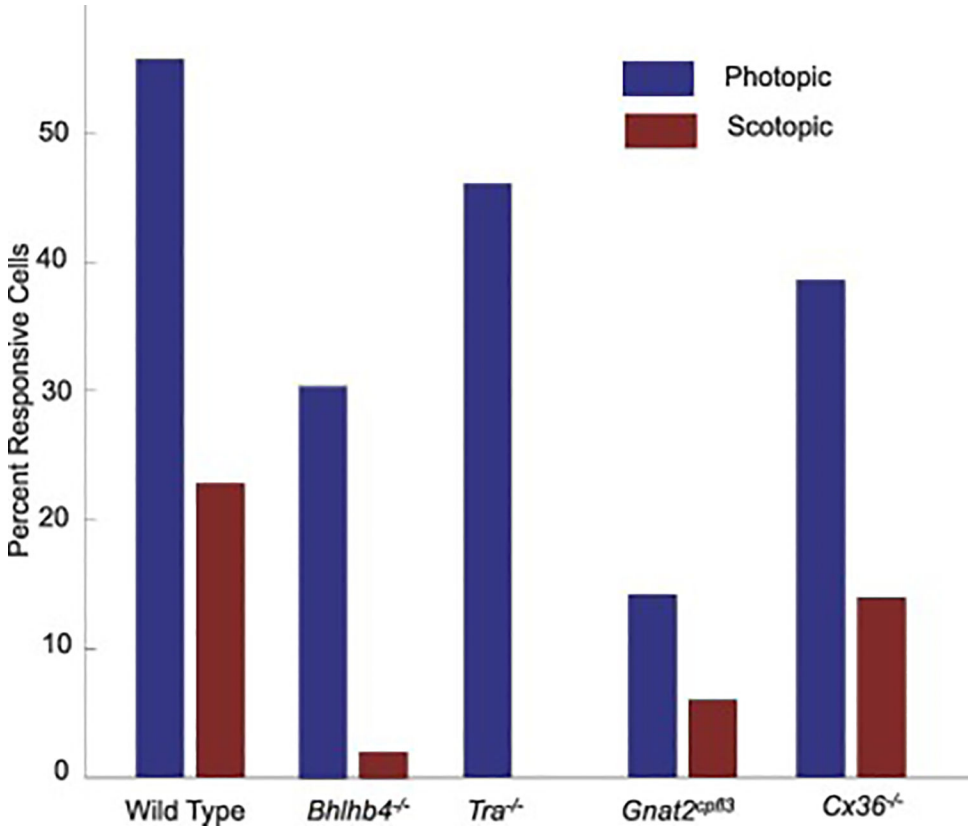

Figure 2.

Percentage of GCs with responsive STAs in *WT*, *Bhlhb4*$^{-/-}$, *Tra*$^{-/-}$, *Gnat2*^{cpfl3} and *Cx36*$^{-/-}$ mice under scotopic and photopic conditions.

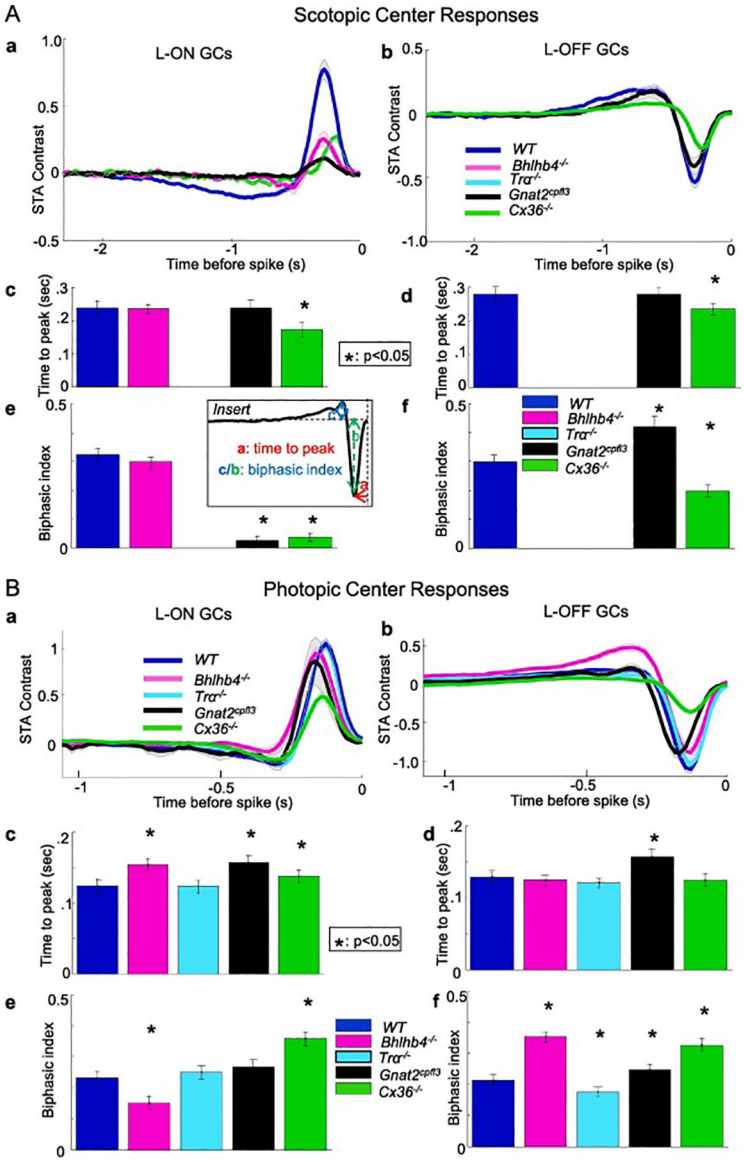

Figure 3.

Mean receptive field center STAs, TTPs and BIs of L-ON GCs and L-OFF GCs in *WT*, *Bhlhb4*$^{-/-}$, *Gnat2*^{cpfl3}, *Tra*$^{-/-}$ and *Cx36*$^{-/-}$ mice under scotopic (A) and photopic (B) conditions. *Tra*$^{-/-}$ mice had no cells with responsive STAs in scotopic conditions. *Bhlhb4*$^{-/-}$ mice had no OFF cells with responsive STAs in scotopic conditions. Mean STAs are shown as thick traces (averaged over numbers of GCs listed in columns 4 and 5 of Table 1, shaded area represents +/− two standard errors) in Figure 3Aa and 3Ba. Figures 3Acd and 3Bcd are the average TTPs (averaged over numbers of GCs listed in columns 4 and 5 of Table 1, TTP values are listed in columns 4 and 5 of Table 2) of L-ON and L-OFF GCs under scotopic and photopic conditions in the five mouse strains. In ON cells, *Bhlhb4*$^{-/-}$ GCs have a longer time-to-peak than wild type (0.154 vs. 0.125 seconds control, p = 2.8e-10, KS test), as did *Gnat2*^{cpfl3} GCs (0.157 vs. 0.125 seconds, p = 1.09e-4, KS test), while *Tra*$^{-/-}$ ON GCs were unaffected. In OFF cells, those from *Gnat2*^{cpfl3} mice had a longer time to peak (−0.157 vs.

−0.129 seconds in control, p = 3.6e-15, KS test), while those from *Bhlhb4*$^{-/-}$, *Tra*$^{-/-}$ and *Cx36*$^{-/-}$ mice showed no difference in TTP. Error bars represent 1 standard deviation. * indicates p< 0.05 (KS test). Figures 3Aef and 3Bef are the average BIs (averaged over numbers of GCs listed in columns 4 and 5 of Table 1, BI values are listed in columns 6 and 7 of Table 2) of L-ON and L-OFF GCs under scotopic and photopic conditions in the five mouse strains. Among ON cells, *Bhlhb4*$^{-/-}$ GCs were significantly less biphasic (0.151 vs. 0.232 in control, p = 1.8e-11, KS test) and *Cx36*$^{-/-}$ GCs are more biphasic. In OFF cells (Figure 3D), those from B4 mice were significantly more biphasic (.354 vs .214, p=7.1e-7, KS test), as were those from *Gnat2*^{cpfl3} and *Cx36*$^{-/-}$ mice (0.247 vs. 0.214, p=.0064, KS test), but those from *Tra*$^{-/-}$ mice were slightly less biphasic (0.177 vs. 0.232 p = .037, KS test). Error bars represent 1 standard deviation. * indicates p< 0.05 (KS test).

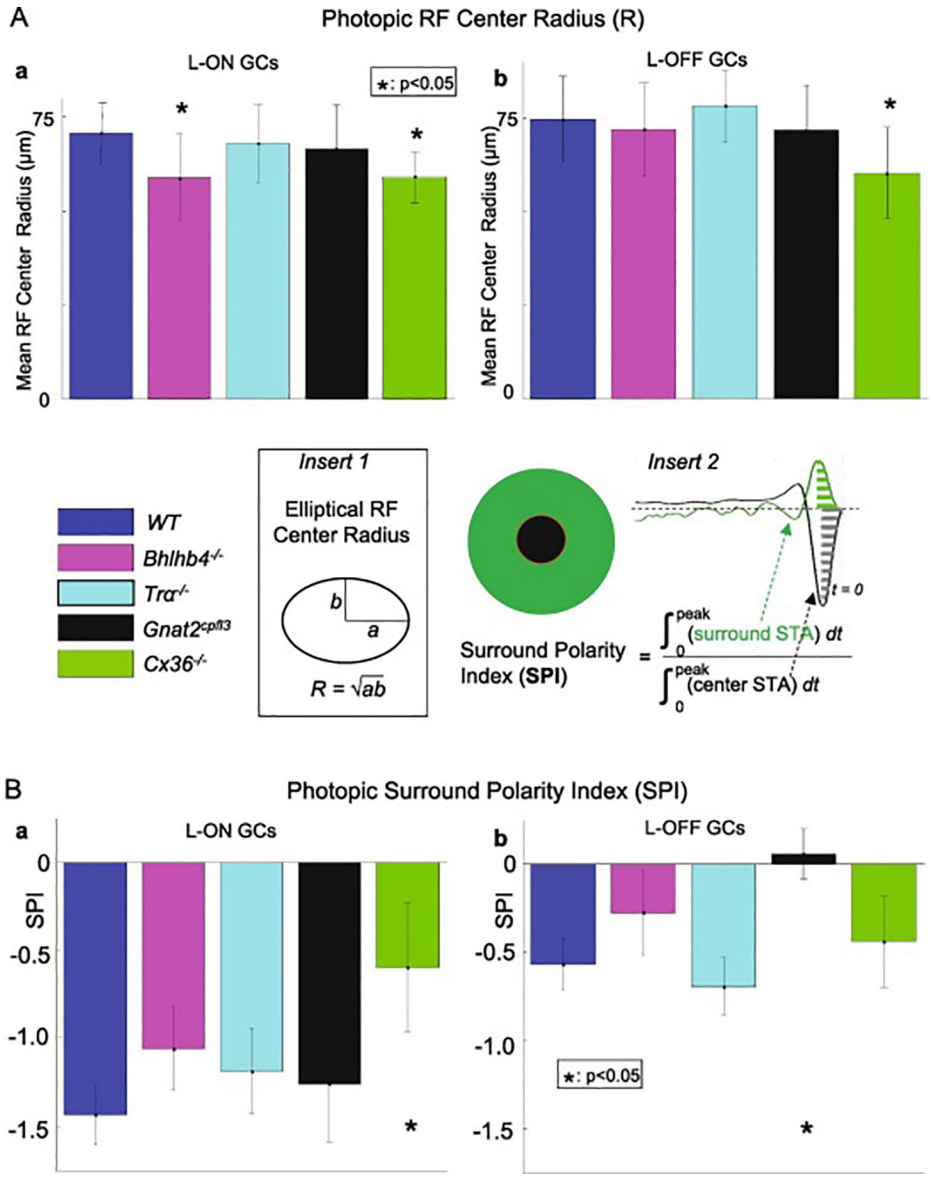

Figure 4.

4Aab are the average RFC radii (R) (averaged over numbers of GCs listed in columns 4 and 5 of Table 1, R values are listed in columns 8 of Table 2) of L-ON and L-OFF GCs under photopic conditions in the five mouse strains. The average RF center radius of ON cells from *Bhlhb4*$^{-/-}$ mice were significantly smaller than those of wild-type mice (64.7 um vs 70.6 um, p =0.018, KS test), while the RF center radius of OFF *Bhlhb4*$^{-/-}$ cells was not significantly different (71.9 um vs. 74.6 um, $p = 0.43$, t-test). The RF center radius of both ON and OFF cells from *Cx36*$^{-/-}$ mice were significantly smaller than those of wild-type mice (64.7 um vs 70.6 um, p =0.018, KS test). Error bars represent 1 standard deviation. * indicates p< 0.05 (Kolmogorov-Smirnov test). Figure 4Bab show the average surround polarity index (SPI) (averaged over numbers of GCs listed in columns 4 and 5 of Table 1, SPI values are listed in columns 9 of Table 2) of L-ON and L-OFF GCs under photopic conditions in the five mouse strains. *Cx36*$^{-/-}$ ON GCs and *Gnat2*^{cpfl3} OFF cells showed

statistically significant increases in SPI (0.006 vs, −0.057 in control, p= 3.9e-4). On the other hand, we found no significant change in SPI for *Bhlhb4*$^{-/-}$ or *Tra*$^{-/-}$ GCs. Error bars represent 1 standard deviation. * indicates p<0.05 (KS test).

Table 1.

Total number of GCs recorded with MEA from N retinas, number and percentage of GCs with responsive STAs, and number of responsive L-ON and L-OFF GCs in *WT*, *Bhlhb4*$^{-/-}$, *Tra*$^{-/-}$, *Gnat2*^{cpfl3} *and Cx36*$^{-/-}$ mice under scotopic and photopic conditions.

Mouse strains (n= # of retinas)	Total Cells	Responsive Cells	Responsive L-ON Cells	Responsive L-OFF Cells
WT (N=15)				
Scotopic	342	78 (23%)	42	36
Photopic	342	191 (56%)	102	89
Bhlhb4$^{-/-}$ (N=9)				
Scotopic	272	5 (1.9%)	5	0
Photopic	272	83 (31%)	50	33
Tra$^{-/-}$ (N=6)				
Scotopic	232	0	0	0
Photopic	232	107 (46%)	47	60
Gnat2^{cpfl3} (N=8)				
Scotopic	310	18 (5.8%)	1	17
Photopic	310	44 (14%)	7	37
Cx36$^{-/-}$ (N=7)				
Scotopic	221	31 (14%)	16	15
Photopic	221	87 (39%)	33	54

Table 2.

Summary of percentages of GCs with responsive STAs, ON and OFF GC TTPs, BIs, RF center radii and SPIs in *WT*, *Bhlhb4*$^{-/-}$, *Tra*$^{-/-}$, *Gnat2*^{cpfl3} *and Cx36*$^{-/-}$ mice under scotopic and photopic conditions. Values measured in WT mice are in bold letters, those in mutant mice that are larger than the corresponding values in WT mice are in red, those that are smaller than the WT values are in blue, and those do not significantly differ from the WT values are in black. "--": measurements are unavailable.

	% rsp. GCs Scot.	% rsp. GCs Phot.	TTP Scot (sec) ON/OFF	TTP Phot (sec) ON/OFF	BI Scot ON/OFF	BI Phot ON/OFF	RF Center Radius (μm) ON/OFF	SPI ON/OFF
WT	**23**	**56**	**0.23/0.28**	**0.12/0.13**	**0.33/0.30**	**0.24/0.22**	**70.8/74.3**	**−1.44/−0.57**
***Bhlhb4*$^{-/-}$** *No R1,C2,C3*	1.9 *	31 *	0.23/--	0.15 */0.12	0.30/--	0.16 */0.36 *	58.8 */71.5	−1.06/−0.28
***Tra*$^{-/-}$** *No R1,R2,R3*	0 *	46 *	--/--	0.12/0.12	--/--	0.26/0.18 *	67.8/77.8	−1.19/−0.70
***Gnat2*^{cpfl3}** *No C1,C2,C3*	5.8 *	14 *	0.23/0.28	0.15 */0.16 *	0.03 */0.40 *	0.27/0.25 *	66.5/72.4	−1.26/+0.06 *
***Cx36*$^{-/-}$** *No R1ON No C3ON No R2,C2,4*	14 *	39 *	0.17 */0.23 *	0.14 */0.12	0.04 */0.20 *	0.36 */0.33 *	59.0 */59.8 *	−0.60 */−0.44

*: p<0.01 (KS test).